physchem

MDPI

Article

A Computational Study of the Mechanism and Kinetics of the 4-Methyl Aniline Reaction with OH Radicals

Tien V. Pham

School of Chemistry and Life Sciences, Hanoi University of Science and Technology, Hanoi 100000, Vietnam; tien.phamvan@hust.edu.vn

Abstract: In this study, the mechanism of the reaction between 4-methyl aniline and hydroxyl free radicals was computed using the M06-2X and CCSD(T) methods, along with the 6-311++G(3df,2p) basis set. The kinetics of the reaction were calculated utilizing the transition state theory and the microcanonical Rice–Ramsperger–Kassel–Marcus theory. The calculated results revealed that NH-C_6H_4-CH_3 was the key product of the system. The total rate coefficient of the system, $k_{\_total} = 2.04 \times 10^{-18}$ $T^{2.07}$ exp[(11.2 kJ/mol)/RT] cm^3/s, was found under the 300–2000 K interval, with P = 760 Torr. At the ambient conditions, the velocity of this reaction was about ten times larger than that of the reaction between $C_6H_5CH_3$ and hydroxyl free radicals, but it was smaller than the aniline + OH rate.

Keywords: 4-methyl aniline; hydroxyl radical; mechanism; kinetics; potential energy surface

1. Introduction

The study of the atmospheric chemistry of organic compounds in the gas phase has attracted considerable interest as a specialized area of research. Due to its significance, particular emphasis is placed on studying the atmospheric interaction between the hydroxyl radical (OH) and organic compounds, particularly aromatic species [1,2].

4-methyl aniline, created from toluene, is mainly used as an intermediate for producing dyes, textiles, plastics, paper, medicines, conducting polymers, and agricultural pesticides [3,4]. Because of its versatility in manufacturing many items, as stated, there is a growing demand for this species [5,6]. Human activities, such as burning garbage, smoking, and fossil fuel combustion, along with natural events like forest fires and volcanic eruptions, are recognized sources of significant 4-methyl aniline emissions into the environment. Many test indicators have shown that 4-methyl aniline is present in the blood and urine of smokers and workers in air-polluted areas [7,8]. Some studies have also shown that, if a person inhales a significant amount of 4-methyl aniline, urinary tract diseases can occur; in more severe cases, it can cause cancer or death [9,10].

Hydroxyl free radicals are known as tropospheric detergents; they can remove most of the volatile organic compounds in this layer [11,12]. Therefore, the reaction of OH radicals with 4-methyl aniline has practical significance in terms of eliminating or minimizing the concentration of 4-methyl aniline in the atmosphere. In the troposphere, the concentration of hydroxyl radicals is relatively significant, standing at about two million molecules per cm^3 [13]. Several investigations have indicated that the temperature and geometric structures of reactants impact the mechanisms of the reactions between aromatic compounds and hydroxyl radicals. in low-temperature regions, the OH addition mechanism in the aromatic cycle is dominant, contrary to the H abstraction mechanism at high-temperature ranges, for example [14–16].

No research has been undertaken, either theoretically or experimentally, on the reaction between 4-methyl aniline and hydroxyl radicals. Thus, the data from the similar reactions of $C_6H_5NH_2$ and $C_6H_5CH_3$ with hydroxyl radicals were utilized for comparison. The $C_6H_5NH_2$ + OH reaction was implemented by various groups. For example, the experimental results of Atkinson and colleagues [17] demonstrated that, at room temperature,

check for updates

Citation: Pham, T.V. A Computational Study of the Mechanism and Kinetics of the 4-Methyl Aniline Reaction with OH Radicals. *Physchem* **2024**, *4*, 146–156. https://doi.org/10.3390/physchem4020011

Academic Editor: Aggelos Avramopoulos

Received: 29 March 2024
Revised: 21 April 2024
Accepted: 24 May 2024
Published: 26 May 2024

the NH_2 hydrogen abstraction and the OH addition are favorable, with the measured rate coefficient being $(1.18 \pm 0.11) \times 10^{-10}$ cm^3/s. This value agrees well with the laboratory numbers of Zetzsch and co-workers [18,19], being about $(1.20 \pm 0.24) \times 10^{-10}$ cm^3/s. In the study of Nahas and colleagues [11], the rate constant of the $C_6H_5NH_2$ + OH system was found to be larger than the available experimental data [17–19], standing at about 4.4×10^{-10} cm^3/s. According to their findings, the abstraction of H from the amino group is significantly less favorable compared to the addition of OH to the aromatic ring. However, their result differs from the theoretical value for the reaction of aniline with a chloride atom, predicted by Chen and colleagues [20]. In their study, the NH_2 hydrogen abstraction dominated compared to the addition of the Cl atom. The rate coefficient of the $C_6H_6CH_3$ + OH system was also determined by various research groups. At 300 K and 100 Torr(He), Fischer and co-workers [21] measured the rate constants of the reactions of benzene + OH and toluene + OH, with the respective values of 1.59×10^{-12} and $(6.11 \pm 0.40) \times 10^{-12}$ cm^3/s. At 304 K, Pitts and colleagues [2] measured the rate coefficients of specific aromatic substances, such as toluene, revealing a value of $(4.15 \pm 1.49) \times 10^{-12}$ cm^3/s. In the range of 250–298 K, Wine and co-workers [22] studied the rate coefficients for the toluene + OH reaction and indicated that they are pressure-dependent. Additionally, at 299 K, Zetzch and colleagues [23] measured the rate coefficients of the OH + toluene reaction, finding a value of 0.2×10^{-12} cm^3/s for the abstraction reaction, whereas there was a measurement of $(7.0 \pm 2.1) \times 10^{-10}$ cm^3/s for the addition reaction. Through computation, Truhlar and co-workers [24] indicated that the abstraction of hydrogen atoms from the methyl group contributes 30%.

To explore the loss of the 4-methyl aniline compound in the atmosphere under the influence of various factors, this present study aims to explore the mechanism and kinetics of the reaction between 4-methyl aniline and OH radicals across a broad range of temperatures (300−2000 K) and pressures (1−7600 Torr).

2. Computational Methods

In this study, the method M06-2X [25,26] and the basis set 6-311++G(3df,2p) [27] were used to calculate the frequencies of the title reaction. This method has been applied for several similar reaction systems [28,29]. The vibrational frequencies of each substance calculated using the above method are the basis for distinguishing transition states from other substances such as intermediate states, reactants, and products. The intrinsic reaction coordinate (IRC) model [30] was also utilized to figure out the relationship between transition states and surrounding points.

The high-cost method known as CCSD(T) [31,32] was employed to compute single-point energies (E_{sp}) for each species on the potential energy surface (PES). Therefore, the total enery of each substance was the sum of E_{sp} and zero-point vibrational energy (E_{zp}), in which E_{zp} was scaled by a 0.971 factor [33–35]. The reason to use the CCSD(T) method is that it gives very accurate results, with an error of only about 4 $kJ \cdot mol^{-1}$ [36,37]. Furthermore, the accuracy of this method was also proved by the values of the T1 diagnostics, presented in Table S1 of the Supporting Information (ESI). The calculated results reveal that both the multireference characteristics and spin contamination are negligible. The copyrighted software, Gaussian version 16 [38], was used for the calculations in this present study.

To calculate rate the constants for the dominant reaction paths of the title reaction, we used the transition state theory (TST) [39] and the microcanonical Rice–Ramsperger–Kassel–Marcus (RRKM) theory [40,41]. Two values, namely, the sum of state (SOS) and density of state (DOS), were calculated based on the activation energies, vibrational frequencies, and moments of inertia. In the process of the computing partition function, the hindered internal rotation (HIR) of the small moieties, including hydroxyl, amino, and methyl, was examined carefully. To solve the master equation and acquire the rate coefficients, dependent on temperature (T) and pressure (P), an energy grain size of 100 cm^{-1} was employed. The epsilon and sigma values for the bath gas and the adduct 4-methyl_aniline_OH used to the compute rate coefficients are 82 K and 3.74 Å [42] and 770 K and 9.2 Å [42], respectively.

The standard form of the "exponential down" model [43] utilizes an average energy transfer per collision, denoted as $<\Delta E_{down}>$, which equals 400 cm^{-1}. Several similar reactions, consisting of C_6H_5 + NH_2 [44] and $C_6H_5NH_2$ + CH_3 [45], use this number as the input parameter for the calculation of rate coefficients. The calculated results are reliable, indicating that this value should be utilized in this study. To verify the reliability of the methods utilized in this study, some thermochemical parameters of the title reaction, such as the energies of enthalpy (ΔH^{o}_{298K}), Gibbs (ΔG^{o}_{298K}), and entropy (ΔS^{o}_{298K}), were also examined and compared with the data from the existing literature. The kinetics of the title reaction were computed by utilizing the software known as Chemrate 1.5.8 [46] and Mesmer 6.1 [47].

3. Results and Discussion

The reaction of 4-methyl aniline with the OH radical, comprising the optimized geometries of all stationary points on the PES, is illustrated in Figure S1 of the Supplementary Materials file. The energy values obtained at different levels (M06-2X and CCSD(T)) are presented in Table 1. The other parameters, such as frequencies, cartesian coordinates, and thermodynamics, are shown in Tables S2–S4 of the Supplementary Materials file, in which the thermochemical data shown in Table S4 indicate that many elementary reaction paths of the title reaction can occur quickly.

Table 1. Single-point energies, zero-point vibrational energies (ZPVE), and relative energies of all species of the title reaction at the two levels.

Species	Single-Point Energies	Single-Point Energies	ZPVE ($kJ \cdot mol^{-1}$)	Relative Energies
	M06-2X (a.u)	CCSD(T) (a.u)		CCSD(T) + ZPVE
(4-methyl aniline + OH)	−400.605	−401.951	1690.69	0.0
CP1	−402.622	−401.959	1711.77	−18
CP2	−402.621	−401.958	1713.49	−15
IS4	−402.646	−401.986	1744.13	−80
IS3	−402.656	−401.991	1756.16	−91
IS2	−402.832	−401.984	1729.10	−80
IS1	−402.837	−401.99	1731.52	−95
T0/4	−402.615	−401.954	1714.44	−4
T0/3	−402.620	−401.957	1720.21	−10
T0/2	−402.614	−401.953	1717.77	1
T0/1	−402.618	−401.955	1718.56	−6
T0P4a	−402.617	−401.955	1692.70	−10.2
T0P4b	−402.617	−401.955	1694.44	−9.8
T0P3	−402.606	−401.943	1660.46	13
T0P2	−402.604	−401.941	1656.87	16
T0P1	−402.611	−401.949	1675.21	1
PR_{4a} + H_2O	−402.652	−401.992	1683.75	−111
PR_{4b} + H_2O	−402.652	−401.992	1683.76	−111
PR_3 + H_2O	−402.621	−401.955	1691.00	−13
PR_2 + H_2O	−402.622	−401.957	1690.88	−16
PR_1 + H_2O	−402.814	−401.993	1675.27	−115

A. The addition of hydroxyl radicals

The addition of OH to the 4-methyl aniline can occur in four directions, as displayed in Figure 1. Among these, the addition of OH to the C-NH_2 carbon atom creates the adduct IS1 and the other additions to the locations of C_2, C_3, and C_4 generate the respective adducts,

namely, IS2, IS3, and IS4. It can be seen from the PES that, at the first step, four addition paths proceed via the well CP1. From the well CP1, the adduct IS1 is formed when the reaction path climbs over the T0/1 transition state. At the location of T0/1, the OH moiety attacks the C_1 atom at a distance of 2.1 Å, where the C_1-OH bond vibrates with a negative frequency of 961i cm^{-1} (see Table S3). Similarly, the adduct IS2 is produced when the reaction path overcomes the hilltop T0/2. It is evident that this transition state represents the highest point when compared to other addition-based transition states like T0/1, T0/3, and T0/4. At the location T0/2, the forming bond C_2-OH is about 2 Å, which is the same as the C_4-OH bond at the point T0/4. However, the negative frequency of the state T0/2 is higher than that of the T0/4 (439i versus 398i cm^{-1}); thus, the C_2-OH bond vibrates stronger than the C_4-OH bond. In contrast to the IS2, the adduct IS3 can be formed more easily because the hilltop T0/3 of this reaction path is the lowest compared to T0/1, T0/2, and T0/4 (see Figure 1). The forming bond C_3-OH of T0/3 vibrates weaker than the bonds C_1-OH, C_2-OH, and C_4-OH due to its longer bond length and smaller negative frequency (~2.2 Å and ~262i cm^{-1}, respectively). The levels of the four adducts depicted on the PES indicate their high stability under typical conditions. While these adducts could potentially contribute to the formation of the final products PR2 or PR3, the reaction pathways involve exceptionally high transition states, which were not included in this investigation.

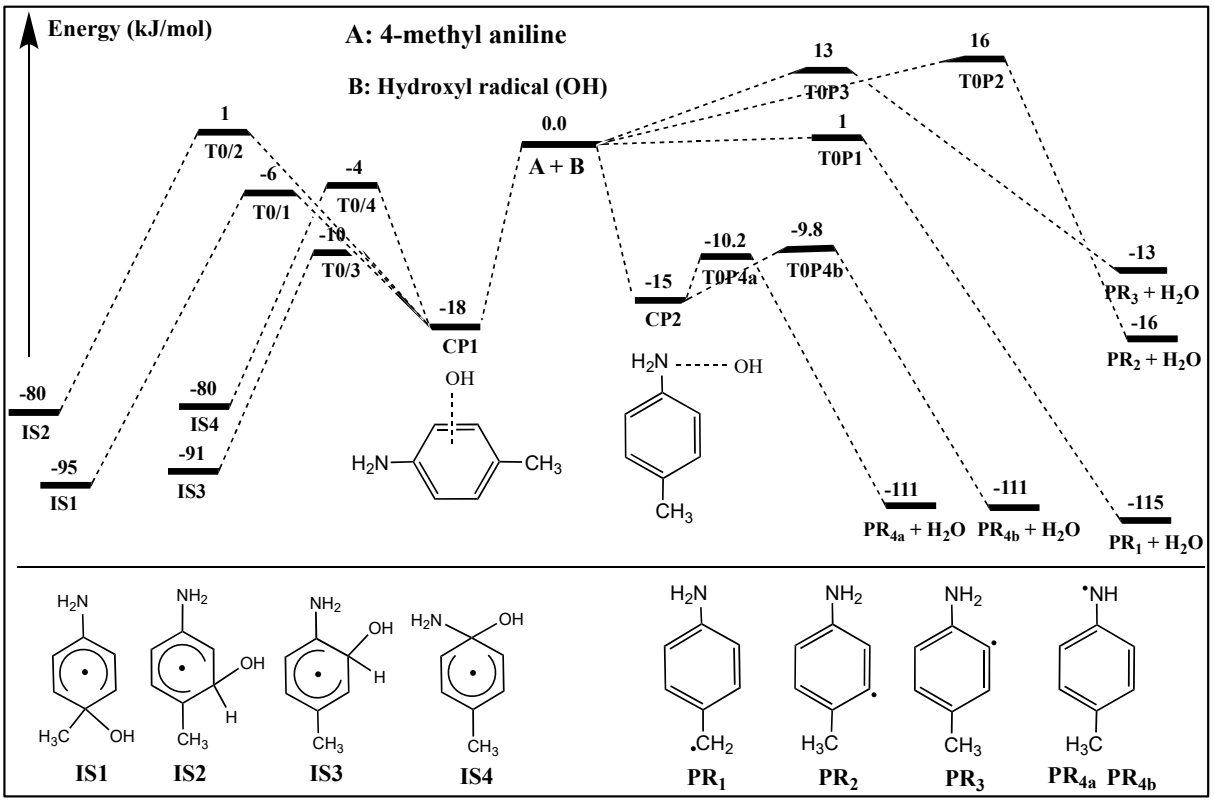

Figure 1. The energies of the key paths of the title reaction are predicted by the CCSD(T) method. The units of energy are kJ/mol.

B. The abstraction of hydrogen atoms

The PES of the reaction reveals that there were five abstraction paths, leading to five different products from PR_1 to PR_4, where the products PR_{4a} and PR_{4b} were produced when the reaction paths proceeded via the well CP2 and two tops of hills T0P4a and T0P4b. It should be noted that T0P4a and T0P4b have the same structures and energy levels (see Figure 1 and Figure S1). Therefore, these two paths should be considered as one reaction path.

As depicted in Figure 1, the H abstraction of the C_3–H bond makes it necessary to surpass the top of hill T0P3, whose barrier height is 13 kJ/mol. The structure of this transition state shows that the lengths of the forming bond H-OH and the breaking bond C_3–H are 1.2 and 1.31 Å, respectively. The negative frequency of the T0P3 is 1078i cm^{-1}, which is suitable for the abstraction of an H atom. In terms of energy, the final product PR_3 is higher than the remaining products of the title reaction. Nevertheless, it can be said that this reaction path still takes place quickly at room temperature. Similarly, the H-abstraction at the C_2 location can occur when the reaction path surpasses the hilltop of T0P2. At this position, the breaking bond C_2–H and the forming bond H-OH were shown to be 1.195 and 1.317 Å, respectively. Their vibrations were characterized by a negative frequency of 1035i cm^{-1}, which was weaker than that of the T0P3 point.

Last but not least, the product PR_1 can be formed by the route going via the low hilltop T0P1 at the level of approximately 1 kJ/mol. It can be seen from the PES that this reaction route is the most exothermic, followed by the direction producing the PR_4 product (115 kJ/mol versus 111 kJ/mol, respectively). It is worth noting that, among the four H-abstraction directions mentioned above, the PR_4 direction is the most dominant, followed by the PR_1 direction. This proves that the H-abstraction from the amino group is more favorable than that from the methyl group.

4. Rate Constant Computations

As shown in Figure 1, eight reaction paths are considered in the kinetics calculation. The four addition paths going from the reactants to IS1, IS2, IS3, and IS4 are denoted as k_1, k_2, k_3, and k_4, respectively, while the four abstraction paths going from the reactants to the products PR1, PR2, PR3, and PR4 are denoted as k_5, k_6, k_7, and k_8, respectively.

In this part, the TST model was used to compute k_1, k_2, and k_3, whereas the RRKM model was utilized to calculate the remaining rate coefficients k_4–k_8. The wide intervals of temperature (from 300 to 2000 K) and pressure (from 1 to 7600 Torr) were considered in these calculations. The calculated results are shown in Tables S5–S10 of the Supplementary Materials file and plotted in Figures 2–7.

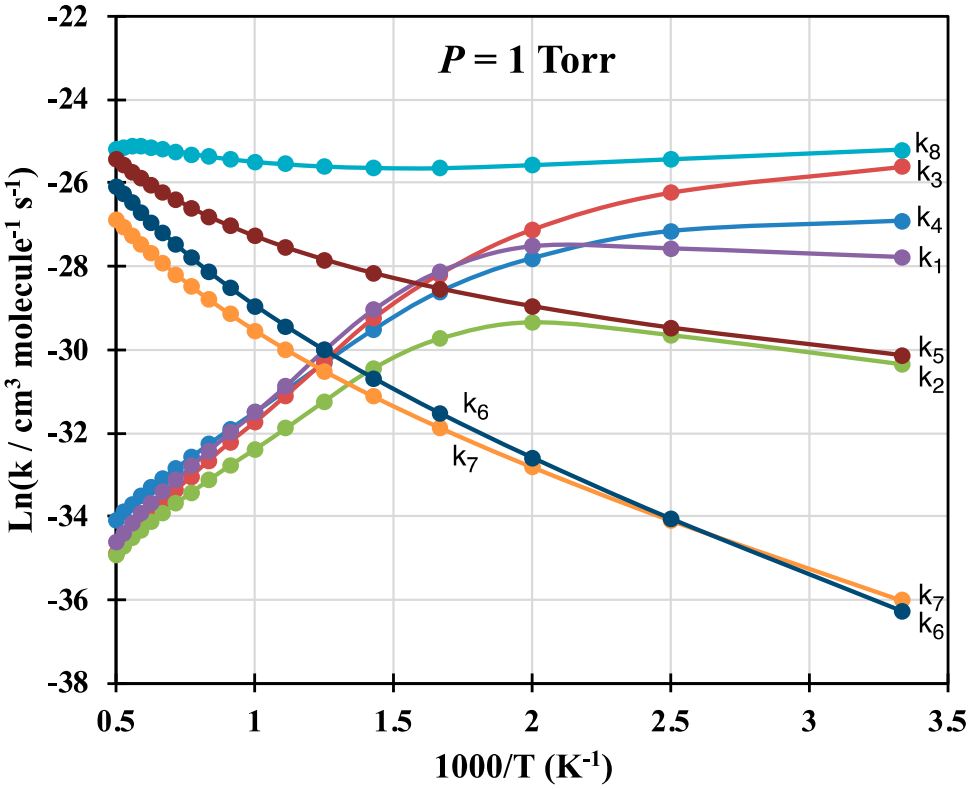

Figure 2. Graph of the k_1–k_8 values under the given temperature range and 1 Torr pressure.

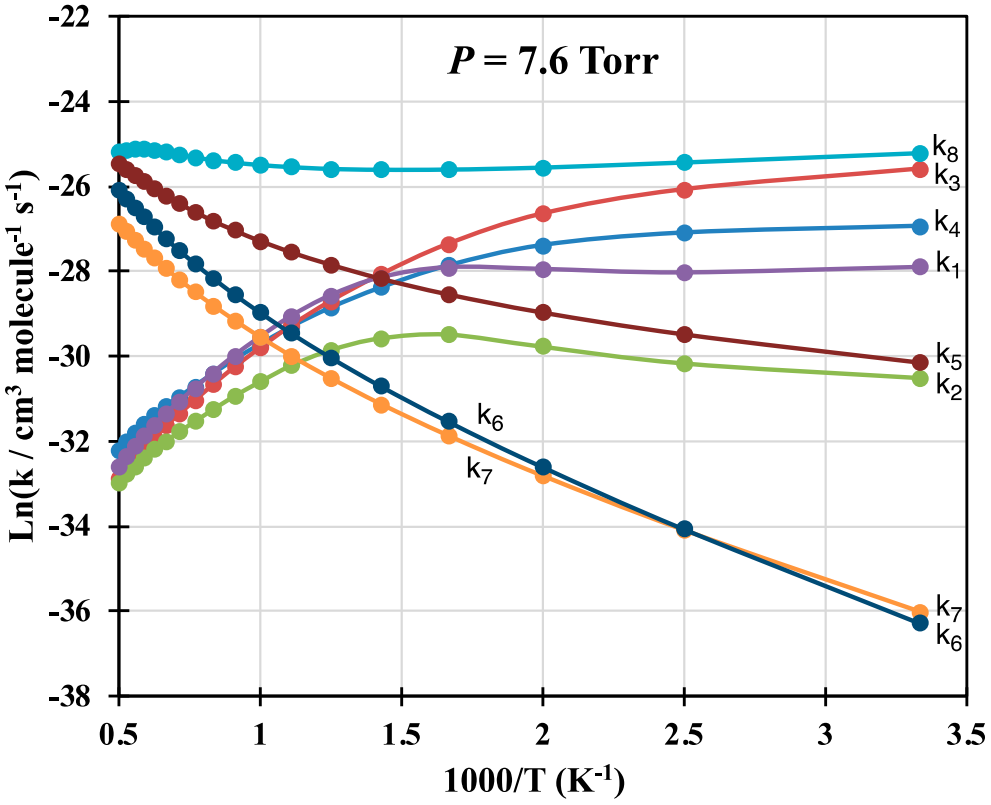

Figure 3. Graph of the k_1–k_8 values under the given temperature range and 7.6 Torr pressure.

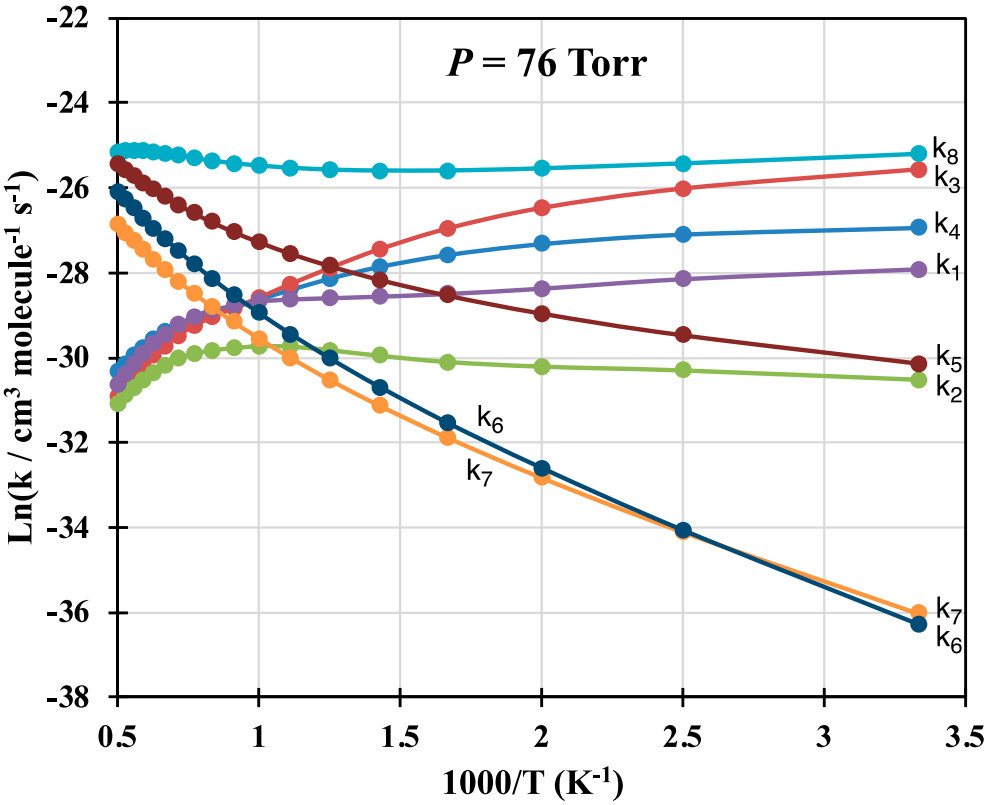

Figure 4. Graph of the k_1–k_8 values under the given temperature range and 76 Torr pressure.

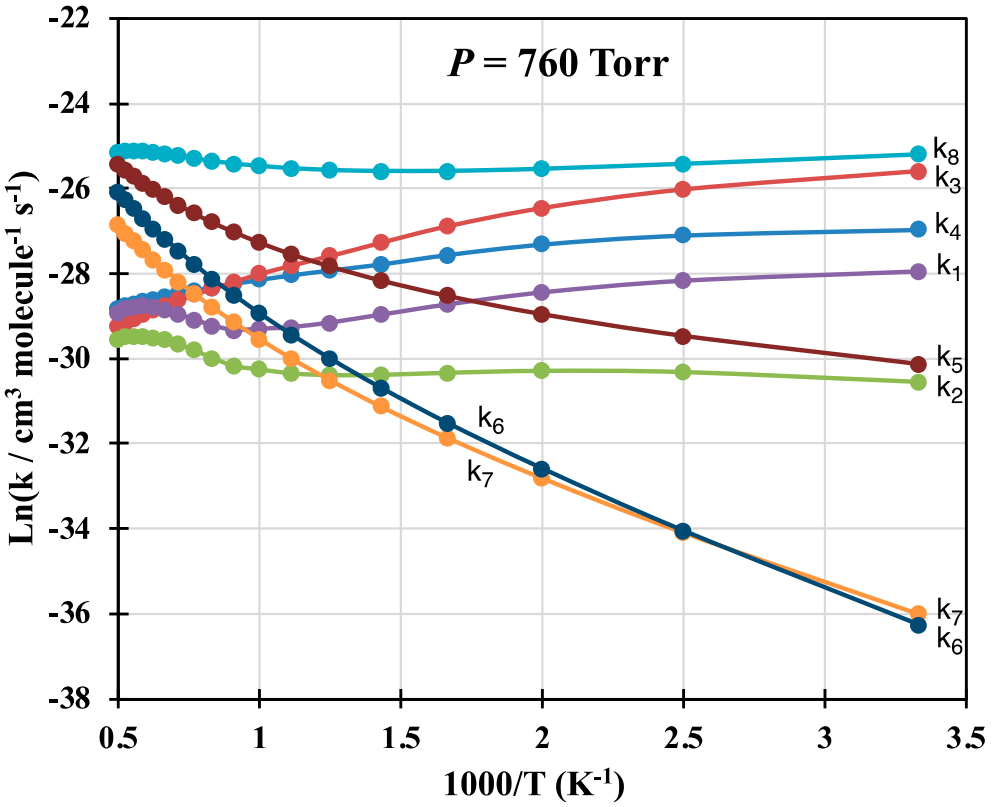

Figure 5. Graph of the k_1–k_8 values under the given temperature range and 760 Torr pressure.

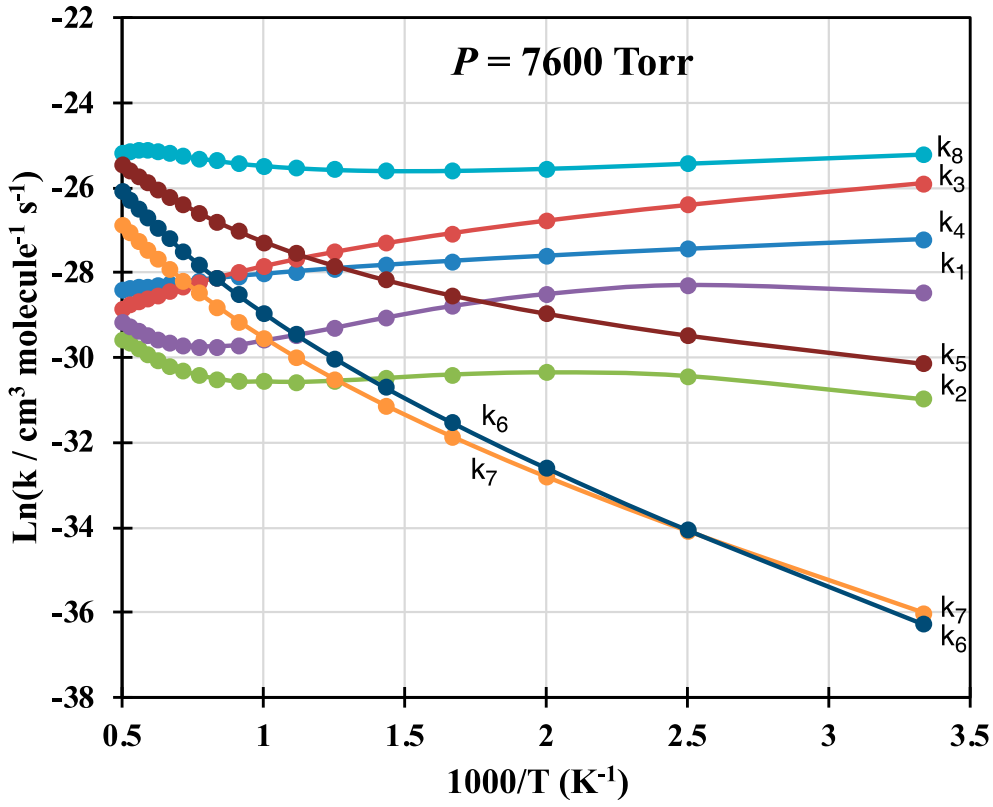

Figure 6. Graph of the k_1–k_8 values under the given temperature range and 7600 Torr pressure.

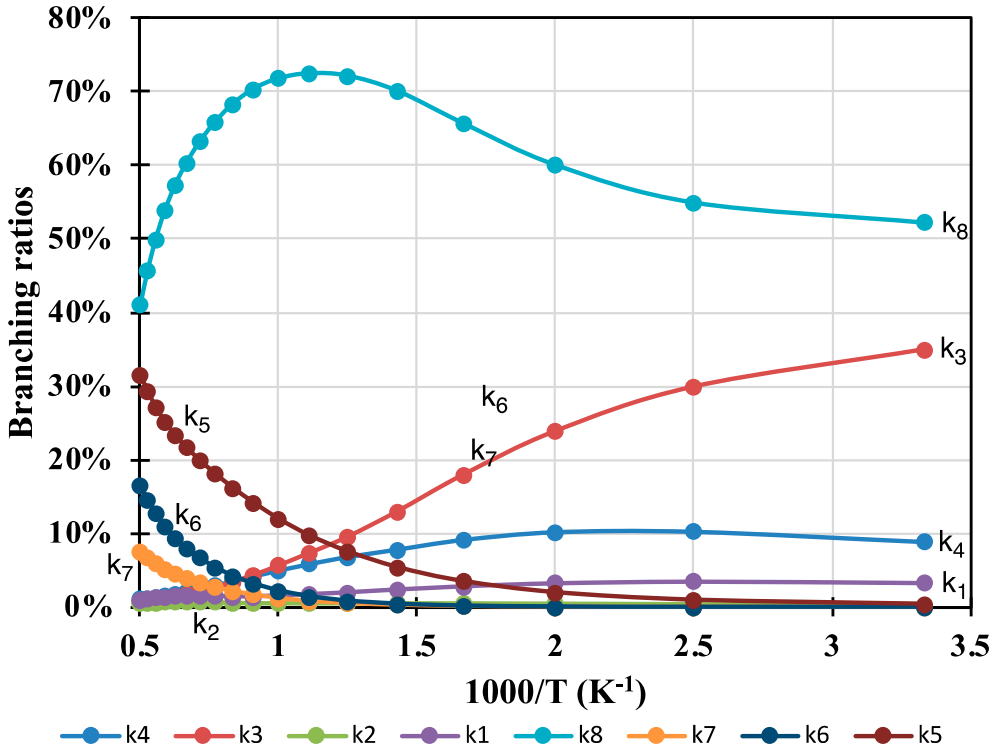

Figure 7. Branching ratios of the k_1–k_8 numbers under the given temperature range and 760 Torr pressure.

Generally, the rate constants of the addition reaction routes are P- and T-dependent, while those of the H-abstraction routes are T-dependent but P-independent. In the considered temperature range, the k_5–k_7 numbers increase significantly, contrary to the decline in k_1–k_4 numbers. Nevertheless, these numbers exhibit a minor rise with rising pressures under the given range. Most notable is k_8, which is almost independent of pressure and temperature and is the most dominant number (see Tables S5–S9).

As shown in Tables S5–S9, the k_3 number is higher than the numbers of k_1 and k_4 under the low-temperature intervals. Conversely, under the high-temperature intervals, these numbers are approximately equal. In addition, in the high-temperature intervals, these values are found to be lower than the numbers of k_5–k_7. The value of k_2 is extremely T- and P-dependent. For example, at a pressure lower than or equal to 76 Torr, this value increases and then rapidly declines, in contrast to its increase at a pressure over 76 Torr. In comparison with the numbers of k_1, k_3, and k_4, the k_2 number is smaller at any temperature or pressure. This is appropriate because the hilltop of T0/2 is remarkably higher than those of T0/1, T0/3, and T0/4 (cf. Figures 2–6).

For the H-abstraction routes, the numbers of k_5–k_7 increase rapidly when the temperature goes from 300 K to 2000 K. They do not depend on pressures, as stated above. Among them, the k_6 number increase most (~1.8×10^{-16}–4.7×10^{-12} cm^3/s), followed by the k_7 number (~2.3×10^{-16}–2.1×10^{-12} cm^3/s). However, these two numbers are still smaller than the k_5 values (~8.1×10^{-14}–8.9×10^{-12} cm^3/s), proving that the PR_1 route is dominant compared to the routes of PR_2 and PR_3. This result agrees well with the calculated energies, as shown on the PES. The total values, $k_{\_total}$ = sum(k_1:k_8), are found to decrease under the low-temperature intervals, but increase gradually under the high-temperature ranges; for example, the 1 Torr value of $k_{\_total}$ reduces in the range of 2.19×10^{-11}–8.69×10^{-12} cm^3/s with T = 300–700 K before going to 2.74×10^{-11} cm^3/s at 2000 K. At room temperature and 760 Torr pressure, $k_{\_total} = 2.16 \times 10^{-11}$ cm^3/s, which is about ten times higher than that of the similar reaction, $C_6H_5CH_3$ + OH [21–25], but it is still lower than the total number of the reaction between $C_6H_5NH_2$ and OH radical [11,17–19]. This outcome indicates that the current reaction occurs at a faster rate than the $C_6H_5CH_3$ +

OH reaction, but at a slower pace compared to the $C_6H_5NH_2$ + OH reaction. At 760 Torr and T = 300–2000K, by using the modified Arrhenius form, the total value is presented as $k_{-total} = 2.04 \times 10^{-18}\ T^{2.07}\ \exp\ [11{,}200/(RT)]\ cm^3/s$.

Branching ratios, shown in Figure 7 and Table S10, reveal that the k_8 value of the route forming the product PR_4 is significantly dominant over the given temperature range. This value increases about 1.4 times in the 300–900 K interval, with a maximum product yield of over 70%, then decreases to well over 40% when the temperature reaches 2000 K. The contribution of the k_3 route over the 300–800 K range is about 34%–10%, whereas the contribution of the k_5 route, from 900 K to 2000 K, is from ~10% to ~32%. In the high-temperature regions, the k_3 contribution declines quickly, contrary to the rise in the k_5 route. The contributions of the routes k_4 and k_6 are also notable, in which the former contributes significantly at low temperatures, and the latter is significant at high temperatures. For the k_7 route, its product yield can go up to nearly 10% at temperatures over 2000 K, but is trivial at temperatures below 1400 K. Lastly, trivial contributions can be seen at the k_1 and k_2 routes, with a total product yield of less than 5%. These calculations demonstrate that the product PR_4 predominates over the specified temperature range and at 760 Torr, with the IS3 adduct prevailing at low temperatures and the product PR_1 doing so at high temperatures.

5. Conclusions

Through studying the reaction routes and the rate constants of the OH + 4-methyl aniline reaction, it can be concluded that the species NH-C_6H_4-CH_3 is the main product of the title reaction in the studied conditions of temperatures and pressures. This product contributes up to over 70% of the reaction, larger than two times of the IS3 adduct and the PR1 product.

Compared with the reactions of toluene and aniline with OH radicals at ambient conditions, the total rate constant of the title reaction is more significant than that of the former. Still, it is smaller than that of the latter. Therefore, it can be said that the rate of removal of organic compounds given above by OH radicals is in the following order: toluene < 4-methyl aniline < aniline.

Supplementary Materials: The following supporting information can be downloaded at: https://www.mdpi.com/article/10.3390/physchem4020011/s1. Table S1: The results of T1 diagnostic analysis calculated at the CCSD(T)/6-311++G(3df,2p) level and spin contamination $<S^2>$ for most of the species on the PES of the 4-methyl aniline + OH system conducted at the M06-2X/6-311++G(3df,2p) level of theory. Table S2: Frequencies of reactants, intermediates, transition states and products of the 4-methyl aniline + OH reaction at the M06-2X/6-311++G(3df,2p) level of theory. Table S3: Optimized coordinates of reactants, intermediates, transition states and products of the 4-methyl aniline + OH reaction at the M06-2X/6-311++G(3df,2p) level of theory. Table S4: Enthalpy changes (ΔH^o_{298K}), Gibbs free energies (ΔG^o_{298K}) and entropies (ΔS^o_{298K}) of the 4-methyl aniline + OH reaction system. Table S5: The bimolecular rate constants (in units of $cm^3\ molecule^{-1}\ s^{-1}$) of the 4-methyl aniline reaction calculated in the range of 300–2000 K and P = 1 Torr (N_2). Table S6: The bimolecular rate constants (in units of $cm^3\ molecule^{-1}\ s^{-1}$) of the 4-methyl aniline + OH reaction calculated in the range of 300–2000 K and P = 7.6 Torr (N_2). Table S7: The bimolecular rate constants (in units of $cm^3\ molecule^{-1}\ s^{-1}$) of the 4-methyl aniline + OH reaction calculated in the range of 300–2000 K and P = 76 Torr (N_2). Table S8: The bimolecular rate constants (in units of $cm^3\ molecule^{-1}\ s^{-1}$) of the 4-methyl aniline + OH reaction calculated in the range of 300–2000 K and P = 760 Torr (N_2). Table S9: The bimolecular rate constants (in units of $cm^3\ molecule^{-1}\ s^{-1}$) of the 4-methyl aniline + OH reaction calculated in the range of 300–2000 K and P = 7600 Torr (N_2). Table S10: Branching ratios of the individual channels of the 4-methyl aniline + OH reaction in the range of 300–2000 K and P = 760 Torr (N_2). Figure S1: Geometries of the reactants, transition/intermediate states and products of the 4-methyl aniline + OH reaction optimized at the M06-2X/6-311++G(3df,2p) level. (Bond lengths are in Å, bond angles are in degs).

Funding: This research received no external funding.

Data Availability Statement: Data is contained within the article and Supplementary Materials.

Acknowledgments: We thank the NCHC in Taiwan for helping us with the calculations.

Conflicts of Interest: The authors declare no conflicts of interest.

References

1. Atkinson, R. Atmospheric Chemistry of VOCs and NO_x. *Atmos. Environ.* **2000**, *34*, 2063–2101. [CrossRef]
2. Doyle, G.L.; Lloyd, A.C.; Darnall, K.R.; Winer, A.M.; Pitts, J.N., Jr. Gas Phase Kinetic Study of Relative Rates of Reaction of Selected Aromatic Compounds with Hydroxyl Radicals in an Environmental Chamber. *Environ. Sci. Technol.* **1975**, *9*, 237–241. [CrossRef]
3. Intisar, A.; Ramzan, A.; Hafeez, S.; Hussain, N.; Irfan, M.; Shakeel, N.; Gill, K.A.; Iqbal, A.; Janczarek, M.; Jesionowski, T. Adsorptive and photocatalytic degradation potential of porous polymeric materials for removal of pesticides, pharmaceuticals, and dyes-based emerging contaminants from water. *Chemosphere* **2023**, *336*, 139203. [CrossRef] [PubMed]
4. Simões, F.R.; Mattoso, L.H.C.; Vaz, C.M.P. Conducting polymers as sensor materials for the electrochemical detection of pesticides. *Sens. Lett.* **2006**, *4*, 319–324. [CrossRef]
5. Nimkar, U. Sustainable chemistry: A solution to the textile industry in a developing world. *Curr. Opin. Green Sustain. Chem.* **2018**, *9*, 13–17. [CrossRef]
6. Vadera, S.; Khan, S. A critical analysis of the rising global demand of plastics and its adverse impact on environmental sustainability. *J. Environ. Pollut. Manag.* **2021**, *3*, 105. [CrossRef]
7. Ge, X.; Wexler, A.S.; Clegg, S.L. Atmospheric amines–Part I. A review. *Atmos. Environ.* **2011**, *45*, 524–546. [CrossRef]
8. Cattaneo, A.; Campo, L.; Iodice, S.; Spinazze, A.; Olgiati, L.; Borghi, F.; Bollati, V. Environmental and biological monitoring of personal exposure to air pollutants of adult people living in a metropolitan area. *Sci. Total Environ.* **2021**, *767*, 144916. [CrossRef] [PubMed]
9. Saeed, A.; Imtiaz, S.; Riaz, S. Study of urinary tract infection in patients suffering from cancer. *J. Cancer Res. Rev. Rep.* **2020**, *2*, 1–15. [CrossRef]
10. Case, R.A. Tumours of the urinary tract as an occupational disease in several industries. *Ann. R. Coll. Surg. Engl.* **1966**, *39*, 213. [PubMed]
11. Abdel-Rahman, M.A.; Shibl, M.F.; El-Demerdash, S.H.; El-Nahas, A.M. Simulated kinetics of the atmospheric removal of aniline during daytime. *Chemosphere* **2020**, *255*, 127031. [CrossRef] [PubMed]
12. Gligorovski, S.; Strekowski, R.; Barbati, S.; Vione, D. Environmental implications of hydroxyl radicals ($^{\bullet}$OH). *Chem. Rev.* **2015**, *115*, 13051–13092. [CrossRef]
13. Gomez Alvarez, E.; Amedro, D.; Afif, C.; Gligorovski, S.; Schoemaecker, C.; Fittschen, C.; Doussin, J.F.; Wortham, H. Unexpectedly high indoor hydroXyl radical concentrations associated with nitrous acid. *Proc. Natl. Acad. Sci. USA* **2013**, *110*, 13294–13299. [CrossRef]
14. Atkinson, R. Gas-phase tropospheric chemistry of organic compounds: A review. *Atmos. Environ.* **1990**, *24*, 1–41. [CrossRef]
15. Kovacevic, G.; Sabljic, A. Atmospheric oxidation of hexachlorobenzene: New global source of pentachlorophenol. *Chemosphere* **2016**, *159*, 488–495. [CrossRef]
16. Atkinson, R.; Aschmann, S.M.; Arey, J.; Carter, W.L. Formation of ring-retaining products from the OH radical-initiated reactions of benzene and toluene. *Int. J. Chem. Kinet.* **1989**, *21*, 801–827. [CrossRef]
17. Atkinson, R.; Tuazon, E.C.; Walllngton, T.J.; Aschmann, S.M.; Arey, J.; Wlner, A.M.; Pitts, J.N. Atmospheric chemistry of aniline, N,N-dimethylaniline, pyridine, 1,3,5-triazine, and nitrobenzene. *Environ. Sci. Technol.* **1987**, *21*, 64–72. [CrossRef]
18. Rinke, M.; Zetzsch, C. Rate constants for the reactions of OH radicals with aromatics: Benzene, phenol, aniline, and 1, 2, 4-trichlorobenzene. Ber. *Bunsenges. Phys. Chem.* **1984**, *88*, 55–62. [CrossRef]
19. Witte, F.; Urbanik, E.; Zetzsch, C. Temperature dependence of the rate constants for the addition of OH to benzene and to some monosubstituted aromatics (aniline, bromobenzene, and nitrobenzene) and the unimolecular decay of the adducts kinetics into a quasi-equilibrium. *J. Phys. Chem.* **1986**, *90*, 3251–3325. [CrossRef]
20. Xie, H.B.; Ma, F.; Yu, Q.; He, N.; Chen, J. Computational Study of the Reactions of Chlorine Radicals with Atmospheric Organic Compounds Featuring NHx-π-Bond (x = 1, 2) Structures. *J. Phys. Chem. A* **2017**, *121*, 1657–1665. [CrossRef] [PubMed]
21. Davis, D.D.; Bollinger, W.; Fischer, S. A Kinetics Study of the Reaction of the OH Free Radical with Aromatic Compounds. 1. Absolute Rate Constants for Reaction with Benzene and Toluene at 300 K. *J. Phys. Chem. A* **1975**, *79*, 293–294. [CrossRef]
22. Tully, F.P.; Ravishankara, A.R.; Thompson, R.L.; Nicovich, J.M.; Shah, R.C.; Kreutter, N.M.; Wine, P.H. Kinetics of the Reactions of Hydroxyl Radical with Benzene and Toluene. *J. Phys. Chem. D* **1981**, *85*, 2262–2269. [CrossRef]
23. Knispel, R.; Koch, R.; Siese, M.; Zetzch, C. Adduct Formation of OH Radicals with Benzene, Toluene, and Phenol and Consecutive Reactions of the Adducts with NOx and O_2. Ber. *Bunsenges. Phys. Chem.* **1990**, *94*, 1375–1379. [CrossRef]
24. Zhang, R.M.; Truhlar, D.G.; Xu, X. Kinetics of the toluene reaction with OH radical. *Research* **2019**, *2019*, 5373785. [CrossRef] [PubMed]
25. Zhao, Y.; Truhlar, D.G. A New Local Density Functional for Main-Group Thermochemistry, Transition Metal Bonding, Thermochemical Kinetics, and Noncovalent Interactions. *J. Chem. Phys.* **2006**, *125*, 194101(1)–194101(18). [CrossRef] [PubMed]
26. Zhao, Y.; Truhlar, D.G. The M06 Suite of Density Functionals for Main Group Thermochemistry, Thermochemical Kinetics, Noncovalent Interactions, Excited States, and Transition Elements. *Theor. Chem. Acc.* **2008**, *120*, 215–241. [CrossRef]

27. Krishnan, R.; Binkley, J.S.; Seeger, R.; People, J.A. Self-consistent molecular orbital methods. XX. A basis set for correlated wave functions. *J. Chem. Phys.* **1980**, *72*, 650. [CrossRef]
28. Nguyen, T.N.; Trang, H.T.T.; Nguyen, N.T.; Pham, T.V. Computational study of the reaction of C_3H_3 with HNCO and the decomposition of C_4H_4NO radicals. *Int. J. Chem. Kinet.* **2022**, *54*, 447–460. [CrossRef]
29. Pan, S.; Wang, L. Atmospheric oxidation mechanism of m-xylene initiated by OH radical. *J. Phys. Chem. A* **2014**, *118*, 10778–10787. [CrossRef]
30. Gonzalez, C.; Schlegel, H.B. An Improved Algorithm for Reaction Path Following. *J. Phys. Chem.* **1989**, *90*, 2154–2161. [CrossRef]
31. Lee, T.J.; Scuseria, G. *Quantum-Mechanical Electronic Structure Calculations with Chemical Accuracy*; Langhoff, S.F., Ed.; Kluwer: Dordrecht, The Netherlands, 1995.
32. Knowles, P.J.; Hampel, C.; Werner, H.-J. Coupled Cluster Theory for High Spin, Open Shell Reference Wave Functions. *J. Chem. Phys.* **1993**, *99*, 5219–5227. [CrossRef]
33. Pham, T.V.; Lin, M.C. A theoretical study on the mechanism and kinetics of the Dimeric TrimethylAluminum+ O_2 reaction in the gas phase: A potential chain-initiation in the hypergolic combustion of TMA in air. *Comput. Theor. Chem.* **2022**, *1212*, 113695. [CrossRef]
34. Pham, T.V.; Lin, M.C. Investigation of product formation in the O (1D, 3P) + N2O reactions: Comparison of experimental and theoretical kinetics. *J. Phys. Chem. A* **2022**, *126*, 1103–1113. [CrossRef]
35. Pham, T.V.; Trang, H.T. Mechanistic and Kinetic Approach on the Propargyl Radical (C_3H_3) with the Criegee Intermediate (CH_2OO). *ACS Omega* **2023**, *8*, 16859–16868. [CrossRef] [PubMed]
36. Helgaker, T.; Klopper, W.; Koch, H.; Noga, J. Basis-set convergence of correlated calculations on water. *J. Chem. Phys.* **1997**, *106*, 9639–9646. [CrossRef]
37. Halkier, A.; Helgaker, T.; Jørgensen, P.; Klopper, W.; Koch, H.; Olsen, J.; Wilson, A.K. Basis-set convergence in correlated calculations on Ne, N_2, and H_2O, Chem. *Phys. Lett.* **1998**, *286*, 243–252.
38. Frisch, M.J.; Trucks, G.W.; Schlegel, H.B.; Scuseria, G.E.; Robb, M.A.; Cheeseman, J.R.; Scalmani, G.; Barone, V.; Petersson, G.A.; Nakatsuji, H.; et al. *Gaussian 16*; Gaussian, Inc.: Wallingford, CT, USA, 2016.
39. Fernandes-Ramos, A.; Miller, J.A.; Klippenstein, S.J.; Truhlar, D.G. Modeling the Kinetics of Bimolecular Reactions. *Chem. Rev.* **2006**, *106*, 4518. [CrossRef] [PubMed]
40. Klippenstein, S.J. Variational optimizations in the Rice–Ramsperger–Kassel–Marcus theory calculations for unimolecular dissociations with no reverse barrier. *J. Chem. Phys.* **1992**, *96*, 367–371. [CrossRef]
41. Wardlaw, D.M.; Marcus, R.A. RRKM Reaction Rate Theory for Transition States of Any Looseness. *Chem. Phys. Lett.* **1984**, *110*, 230–234. [CrossRef]
42. Hippler, H. Collisional deactivation of vibrationally highly excited polyatomic molecules. II. Direct observations for excited toluene. *J. Chem. Phys.* **1983**, *78*, 6709. [CrossRef]
43. Tardy, D.C.; Rabinovitch, B.S. Collisional Energy Transfer. Thermal Unimolecular Systems in the Low-Pressure Region. *J. Chem. Phys.* **1966**, *45*, 3720–3730. [CrossRef]
44. Pham, T.V.; Trang, H.T. Reactions of Methyl Radicals with Aniline Acting as Hydrogen Donors and as Methyl Radical Acceptors. *ACS Omega* **2023**, *8*, 17005–17016. [CrossRef] [PubMed]
45. Pham, T.V.; Tran, A.V. Gas Phase Reaction of Isocyanic Acid: Kinetics, Mechanisms, and Formation of Isopropyl Aminocarbonyl. *ACS Omega* **2021**, *6*, 34661–34674. [CrossRef] [PubMed]
46. Mokrushin, V.; Bedanov, V.; Tsang, W.; Zachariah, M.; Knyazev, V. *ChemRate*; Version 1.5.8; NIST: Gaithersburg, MD, USA, 2009.
47. Glowacki, D.R.; Liang, C.H.; Morley, C.; Pilling, M.J.; Robertson, S.H. MESMER: An open-source master equation solver for multi-energy well reactions. *J. Phys. Chem. A* **2012**, *116*, 9545–9560. [CrossRef] [PubMed]